Int. J Med. Pharm. Res. (P-ISSN: 2958-3675 | E-ISSN: 2958-3683)
Available on: https://ijmpr.in/

International Journal
of Medical and
Pharmaceutical Research

ORGINAL ARTICLE **OPEN ACCESS**

In cases where cardiomyocytes generated from stem cells are substituted, myosin activity and a contractile process effectiveness are modified

Bijay Hansda[1], MD Faiz Afzal[2], Suyash Saurabh[3], Ajitabh Ranjan[4]
[1-4]Junior Resident, Physiology Department, Rajendra Institute of Medical Sciences, Bariatu, Ranchi, Jharkhand, India 834009

OPEN ACCESS

***Corresponding Author**
Bijay Hansda
Junior Resident, Physiology Department, Rajendra Institute of Medical Sciences, Bariatu, Ranchi, Jharkhand, India 834009

Received: 13-01-2025
Accepted: 19-02-2025
Available online: 28-02-2025

A B S T R A C T

Contractile function is primarily determined by the myosin heavy chain (MyHC). The β-isoform is the most often expressed in human ventricular cardiomyocytes (CMs). We previously showed that following long-term incubation on glass coverslips covered with laminin, approximately 80% of human embryonic stem cell-derived cardiomyocytes (hESC-CMs) express just β-MyHC. In order to characterise cellular function, we examined the effects of enzymatically separating hESC-CMs following prolonged growth and then replating them. In a micro-mechanical setting, we found that force-related kinetic characteristics reflected variations in calcium transients and resembled α- rather than β-MyHC-expressing myofibrils. According to single-cell immunofluorescence analysis, replating hESC-CMs caused α-MyHC to be rapidly up-regulated, as evidenced by increases in hESC-CMs that expressed α-MyHC solely and α/β-MyHC mixed. Individual CMs generated from human induced pluripotent stem cells (hiPSCs) similarly showed a similar increase in the variability of MyHC isoform expression following replating. During the second week following replating, the alterations in cardiomyocyte function and MyHC isoform expression brought on by replating were reversible. The expression profile of genes and pathways relevant to mechanosensation/transduction, particularly integrin-associated signaling, changed, according to gene enrichment analysis based on RNA-sequencing data. Thus, focal adhesion kinase (FAK), an integrin downstream mediator, enhanced β-MyHC expression on a rigid matrix, thereby confirming gene enrichment analysis. In conclusion, long-term cultivated human stem cell-derived CMs underwent significant changes in gene expression, MyHC isoform composition, and function as a result of detachment and replating. This led to changes in mechanosensation/transduction, which should be taken into account, especially for subsequent in vitro tests.

Keywords: Cardiomyocytes, Myosin Activity, Stem Cell Differentiation

INTRODUCTION

MYH7 encodes β-MyHC, which is mostly expressed by human adult ventricular CMs, while MYH6 encodes α-MyHC, which is primarily expressed by atrial CMs (Reiser et al., 2001). The primary factor influencing the heart's contractility and power output is the expression of the Myosin heavy chain (MyHC) isoform (Herron and McDonald, 2002; Palmiter et al., 1999; Schwartz et al., 1981). CMs with a higher amount of α-MyHC have faster myocardial contraction speed (Schwartz et al., 1981), peak normalised power output (Herron and McDonald, 2002), and faster cross bridge kinetics (Rundell et al., 2005). These findings are linked to a higher ATPase activity of α-MyHC. According to Yang et al. (2014), human pluripotent stem cell-derived cardiomyocytes (hPSC-CMs) hold significant promise for therapeutic uses in pharmacological research, regenerative medicine, and as models for cardiac illness or cardiomyocyte development. Despite significant advancements in differentiation techniques, it has been demonstrated that the phenotype of hPSC-CMs differs significantly from adult human CMs in terms of gene expression, morphology, and function (Denning et al., 2016). One of numerous distinct techniques to promote in vitro maturation of hPSC-CMs is long-term culture on a rigid matrix (Yang et al., 2014). We previously demonstrated that after a prolonged culture on laminin-coated glass coverslips, or a stiff matrix, the number of human embryonic stem cell–derived car-diomyocytes (hESC-CMs) that express only the β-isoform of MyHC rises to over 80%, whereas no CMs that express only α-MyHC were detected (Weber et al., 2016). Only around 10% of CMs that are grown in a soft environment as cardiac bodies (CB) in suspension culture for the same amount of time exhibit only β-MyHC, whereas the majority express α-MyHC (Weber et al., 2016). The development of

hESC-CMs to a rather homogenous culture with ventricular phenotype in terms of the degree of MyHC isoform expression is thus encouraged by long-term culture on a stiff matrix. However, in addition to morphological and functional traits, the expression of additional genes also influences the maturation stage of hPSC-CMs (Jiang et al., 2018). However, following short-, middle-, or long-term culture, CMs are frequently separated from their substrate and quickly replated for additional analysis in models for cardiac illness or cardiomyocyte development (Yang et al., 2014). Our goal was to find out if hESC-CM function is affected by enzymatically removing and replacing hESC-CMs. Gene expression and cell function may be significantly impacted when cells separate from the substrate. Detachment, for instance, has been demonstrated to affect signaling pathways that control contractile activity during cell migration (Ren et al., 2004).

Furthermore, it has been shown that the recovery and viability of hiPSC-CMs were affected differently by various combinations of the replating matrix and detachment chemicals (Koc et al., 2021). A change in the matrix's rigidity is thought to be connected to the detachment and replating of CMs. Cardiomyocyte remodeling under healthy and pathological situations is known to result from adaptations to a changed mechanical environment in vivo, which are mediated via cellular mechanosensation/transduction and its downstream effects (Saucerman et al., 2019). Integrins have been demonstrated to be essential for mechanotransduction in CMs by connecting intracellular signals to the extracellular matrix (ECM) (Israeli-Rosenberg et al., 2014; Pentassuglia and Sawyer, 2013). Focal adhesion kinase (FAK) is an essential downstream mediator of integrins in the control of cardiac cell–cell and cell–matrix interactions. A number of mechanisms contribute to additional downstream integrin/FAK signaling, including the extracellular signal-regulated kinase (ERK) 1/2, a member of the mitogen-activated protein kinases (MAPKs). FAK and integrins have been demonstrated to be involved in the differentiation of induced pluripotent stem cells into CMs and to play significant roles in cardiac development and disease (Castillo et al., 2020; Santoso et al., 2019). Evaluation of the MyHC isoform expression profile of replated human induced pluripotent stem cell-derived (hiPSC) CMs and replated hESC-CMs revealed a fairly quick switch from β- to α-MyHC expression. This change was linked to functional adjustments. In the second week following replating, it was demonstrated that changes in MyHC isoform expression and contractile performance were reversible. Additionally, replated hESC-CMs showed changes in the expression of genes linked to mechanosensation/transduction, particularly integrin-associated signaling. Similarly, β-MyHC expression was reduced by blocking the integrin downstream mediator FAK. After hPSC-CMs detach and rep-late, changes in mechanosensation/transduction may cause changes in MyHC isoform expression and CM function, according to changes in gene expression, particularly of integrin-associated signaling pathways.

MATERIALS AND METHODS

hESC-CMs' differentiation, genetic cardiomyocyte enrichment, and culture

As previously reported, hESC-CMs were differentiated, genetically enriched, and cultivated (Fig. 1; Schwanke et al., 2014; Weber et al., 2016; Xu et al., 2008). In summary, Collagenase B (Roche) was used to dissociate suspension-derived CBs between days 12 and 20. PBS (without Ca2+ and without Mg2+; Gibco) was used to wash the CBs. They were then treated with Collagenase B (1 mg/ml) in a low-calcium solution (Maltsev et al., 1994; 120 mM NaCl; 5.4 mM KCl; 5 mM MgSO4*7 H2O; 5 mM Na-pyruvate; 20 mM glucose; 20 mM taurine; 10 mM HEPES/NaOH; and 30 µM (3 µg/ml) CaCl2; pH: 6.9 at room temperature) for about 30 minutes at 37°C with gentle stirring until a single-cell solution was achieved. As an alternative, CMs were separated using the STEMCELL Technologies StemDiff Kit (5 min, 37°C, with mixing at 1,000 rpm). The isolated cells were re-suspended in IMDM Glutamax (Gibco, Thermo Fisher Scientific) with 10 µM Rho-associated protein kinase (ROCK)-inhibitor Y-27632 (Tocris) and 10% fetal calf serum (FCS; GE Healthcare Life Science) added. Resuspended CMs were grown for an additional 35–69 days after being plated onto glass coverslips coated with laminin (40 µg/ml; Life Technologies, Thermo Fisher Scientific). Dulbecco's modified Eagle's medium (DMEM; high glucose, pyruvate, no glutamine; Life Technologies, Thermo Fisher Scientific) was substituted for the basic serum-free (bSF)-only medium after one day.

2 mmol/liter L-glutamine, 1% non-essential amino acids (Gibco, Thermo Fisher Scientific), 100 U/ml penicillin-streptomycin (Gibco, Thermo Fisher Scientific), 0.1 mmol/liter β-mercaptoethanol, 17 µg/ml sodium selenite, 11 µg/ml transferrin, and 10 µg/ml human insulin (all Sigma-Aldrich, Merck) are added, and it is replaced twice a week. A transgenic hES3 αMyHCneoPGKhygro line with a Neomycin selection marker regulated by the CM-specific αMyHC-promotor was employed to enrich for CMs (Schwanke et al., 2014). To create a nearly pure CM population, 200 µg/ml G418 (Gibco, Thermo Fisher Scientific) was introduced during the first seven days of hESC-CM cultivation on glass coverslips covered with laminin. For replating, hESC-CMs were treated with either 500 µl Accutase (Gibco, Thermo Fisher Scientific) per coverslip for 5 minutes at 37°C (days 34, 35, and 42) or 200 µl Collagenase B (1 mg/ml) in low calcium solution (Maltsev et al., 1994) per coverslip for 30 minutes at 37°C (days 42, 45, 48, and 55). On laminin-coated glass coverslips, dissociated hESC-CMs were reseeded in IMDM Glutamax supplemented with 10% FCS and 10 µM ROCK-inhibitor Y-27632 for 23 hours. They were then cultured in bSF-only media (Fig. 1). hESC-CMs grown on laminin-coated glass coverslips were treated with or without 5 µM FAK-inhibitor 14 (Santa Cruz Biotechnology) dissolved in ethanol or DMSO, or with 10 µM MEK1/2 inhibitor U0126 (Cell Signaling) dissolved in DMSO, starting on day 7 and lasting for two days in pharmacological interference experiments. Furthermore, hESC-CMs cultured on

Matrigel-coated (Corning) polydimethylsiloxane (PDMS; Specialty Manufacturing, Inc.) coverslips were treated with or without 10 µM MEK1/2 inhibitor U0126 or 5 µM FAK inhibitor 14 for two days till day 35.

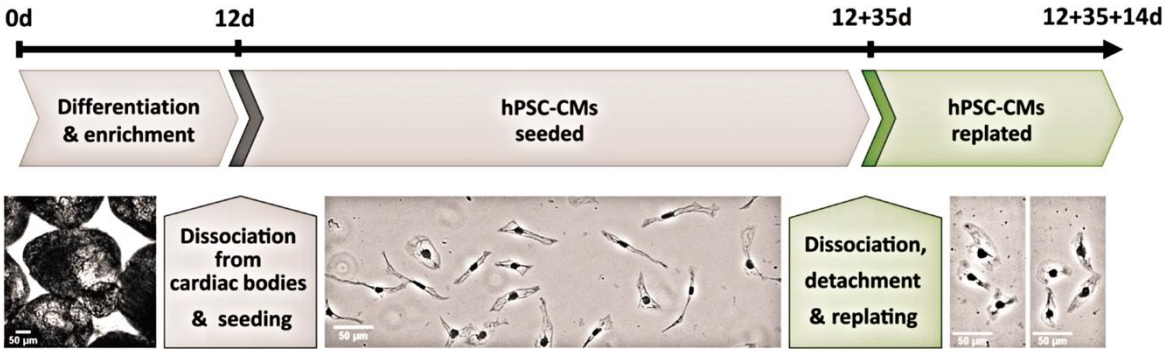

Figure 1 : Overview of hPSC-CM differentiation, enrichment, seeding, and replating on glass coverslips coated with laminin, a rigid matrix. On the designated days, hPSC-CMs underwent differentiation, enrichment, seeding, and replateing.

Differentiation and cultivation of hiPSC-CMs

HiPSC-CMs (Chatterjee et al., 2021; Haase et al., 2017; Kreutzer et al., 2022) were cultured and differentiated into CMs using wild-type hiPSC-CMs Phoenix, and then purified using a previously described modified methodology. In summary, differentiation was started at 75–80% confluency using 5 µM CHIR99021 (Merck) in cardio differentiation medium (500 ml RPMI 1640 medium, GlutaMAX Supplement, HEPES [Life Technologies], 250 mg human recombinant albumin [Sigma-Aldrich], and 100 mg L-ascorbic acid 2-phosphate sesquimagnesium salt hydrate [Sigma-Aldrich]) in 12-well plates (Greiner) coated with Geltrex (Invitrogen, Thermo Fisher Scientific). Fresh medium containing 5 µM IWP2 (Selleck) was added after 48 hours. Every 48 hours, the medium was switched out. The cells began to spontaneously contract on the eighth day of differentiation. Cells were kept in cardiac culture medium (500 ml RPMI 1640 medium, GlutaMAX Supplement, HEPES [Life Technologies], 10 ml B-27 Supplement [50X], serum free [Life Technologies]) from this point on, with a medium change occurring every two days. Cells were separated and planted into T25 flasks (Corning) on day 15. To summarize, cells were treated with 5X Trypsin-EDTA (Life Technologies, Thermo Fisher Scientific) in PBS for 5 minutes at 37°C after being cleaned with Versene (Life Technologies, Thermo Fisher Scientific). Before being resuspended in cardio digestion medium (80 ml Cardio Culture Medium, 20 ml heat-inactivated FBS [Life Technologies, Thermo Fisher Scientific], and 100 µl thiazovivin [Selleck]), cells were collected and centrifuged at 200 × g for five minutes at room temperature.

A density of 500,000 cells per T25 flask covered with 0.1% gelatin was used for cell seeding. To further enrich CMs, the medium was switched to cardio selection medium (500 ml RPMI 1640 [without glucose, without HEPES; Life Technologies, Thermo Fisher Scientific], 250 mg human recombinant albumin, 100 mg L-ascorbic acid 2-phosphate sesquimagnesium salt hydrolyte, and 2 ml sodium DL-lactate solution [60%, wt/wt; Sigma-Aldrich] in HEPES [Sigma-Aldrich]) for seven days. After that, the media was switched back to cardiac culture medium until day 46, at which point the cells were once more dissociated using the previously mentioned protocol.

CMs were seeded at a density of 100,000 cells on 18 mm glass coverslips coated with laminin for immunostaining. CMs were seeded at a density of 200,000 cells on 32-mm laminin-coated glass coverslips in order to analyze protein expression. Cardio culture media was used to develop the cells till days 64 or 66. Trypsin-EDTA was applied to a fraction of 64-d (= 18 d on laminin-coated glass coverslips)-old cells for 5 minutes at 37°C in order to replate them. The separated cells were then replated on glass coverslips coated with laminin and cultured in cardiac digestion mixture for a further two days. Cells were either fixed with 4% paraformaldehyde (Merck) for immunostaining or lysed for protein expression investigation on day 66 (see below).

Analysis of MyHC and MLC isoform expression by immunofluorescence.

As previously described (Weber et al., 2016, 2020), single hESC-CMs were immunostained using particular primary antibodies against α-MyHC (rabbit, polyclonal, α-huMYH6) and β-MyHC (mouse, monoclonal, M8421; Sigma-Aldrich, Merck). Secondary anti-rabbit Alexa Fluor 488 (goat, polyclonal, A11008; Thermo Fisher Scientific) for α-MyHC and anti-mouse Alexa Fluor 555 antibodies (goat, polyclonal, A21422; Thermo Fisher Scientific) for β-MyHC. Specific primary anti-bodies against MLC2a (mouse, monoclonal, 311 011; Synaptic Systems) and MLC2v (rabbit, polyclonal, 10906-1-AP; Pro-teintech) were employed for myosin regulatory light chain (MLC2) isoforms. Secondary anti-mouse Alexa Fluor 555 (donkey, polyclonal, A31570; Thermo Fisher Scientific) was used for MLC2a, and anti-rabbit Alexa Fluor 488 (donkey, polyclonal, A21206; Thermo Fisher Scientific) was used for MLC2v. The nuclear counterstain

employed was DAPI (Sigma-Aldrich). Each experiment used the same anti-body dilutions and staining times. Imaging was done using either an Olympus IX51 fluorescence microscope (Olympus) with an Olympus LCAch N Phase 20×/ 0.40 NA Php or Olympus LCAch 40×/0.55 NA Php objective lens, and filter sets for DAPI (BP330-385, ET460/50M; Chroma), GFP (HQ470/40X, HQ525/50M; Chroma), and Cy3 (HQ546/11X, HQ585/40M; Chroma), or an Olympus IX83 fluorescence mi- croscope with an Olympus LUCPlanFL N 20×/0.45 NA or Olympus UPlanFl 40×/0.75 NA Ph2 objective lens and a cooled CCD camera (Orca-R2; Hamamatsu Photonics), using filter sets for DAPI (AT350/50X, ET460/50M, T400LP; Chroma), GFP (ET470/40X, ET525/50M, T495LPXR; Chroma), and Cy3 (ET545/25X, ET605/70M, T565LPXR; Chroma).

Greyscale images of CMs were captured with the same exposure periods for either MLC2a and MLC2v specific channels or α-MyHC and β-MyHC. Using the original, unaltered picture files, the myosin isoform expression of individual CMs was classified and scored based only on sarcomere staining, as previously explained (Weber et al., 2016, 2020). The fractions of cells in the various categories were allocated for single-cell IF in accordance with the previously mentioned protocol (Weber et al., 2020).

Different types of myosin

Green: α, exclusively α-MyHC expressing CMs; orange: β > α, co-expression of α- and β-MyHC with higher level of β-MyHC fluorescence; yellow: α = β, coexpression of α- and β-MyHC with equivalent fluorescence levels; α > β: light green, coexpression of α- and β-MyHC with higher level of α-MyHC fluorescence; and green: α, exclusively α-MyHC expressing CMs.

MLC2 isoforms

Dark blue: v = a, coexpression of MLC2v and MLC2a with equivalent fluorescence levels; a > v: light blue, coexpression of MLC2v and MLC2a with higher level of MLC2a fluorescence; cyan: MLC2a, exclusively MLC2a expressing CMs; blue: v > a, coexpression of MLC2v and MLC2a with higher level of MLC2v fluorescence; and magenta: MLC2v, exclusively MLC2v expressing CMs.

Analysis of protein expression

Plated hPSC-CMs were lysed in kinase buffer (20 mM Tris-acetate, pH 7.0; 0.1 mM EDTA; 1 mM EGTA; 1 mM Na3VO4; 10 mM β-glycerolphosphate; 50 mM NaF; 5 mM pyrophosphate; 1% Triton X-100; 2 µg/ml leupeptin), supplemented with Protease Inhibitor Cocktail [Bimake] and Phosstop Phosphatase Inhibitor Cocktail [Roche], in order to analyze sarcomeric proteins. RotiLoad1, 4× conc. (Roth), and lysates were combined (4:1) for loading. Adult human atrial and ventricular samples were made as natural tissue controls. MyHC detection using SDS-PAGE gels (8% SDS with 5% glycerol) was carried out in accordance with earlier instructions (Iorga et al., 2018; Kraft et al., 2013). (phospho-)FAK and (phospho-)ERK1/2 were detected using hESC-CM samples that were produced as previously mentioned. After proteins were separated using SDS-PAGE (10% SDS gel), they were put onto a nitrocellulose blotting membrane (0.22 µm) and blocked using 5% milk powder (Santa Cruz) diluted in 0.1% Tween 20 (TBS-T; Sigma-Aldrich) and Tris-buffered saline (TBS). Primary antibodies were incubated in TBS-T at 4°C for the entire night in order to detect the presence of either β-tubulin (mouse, monoclonal, G098; Applied Biological Materials Inc.), phospho-FAK (rabbit, polyclonal, 3283; Cell Signaling), ERK1/2 (rabbit, polyclonal, 9102; Cell Signaling), or phospho-ERK1/2 (rabbit, polyclonal, 9101; Cell Signaling). For one hour at room temperature, secondary antibodies against rabbit (from goat, 1706515; Bio-Rad) or mouse (from goat, 1721011; Bio-Rad) were incubated in TBS-T. Enhanced chemiluminescence was used to acquire Western blot images using an ImageQuant LAS 4000 imaging system (GE Healthcare).

Evaluation of the sub-cellular myofibrils' ability to contract

As previously described (Iorga et al., 2018), intracellular myofibrils were made available after the chemical demembranation of replated (2, 3, 6, 7, 8, 9, and 10 d) or non-replated (35 d) hESC-CMs. Consequently, a thin myofibrillar bundle was affixed between a stiff needle and a nN-sensitive force probe in a myofibrils micromechanical setup. Sarcomere lengths (SL) of myofibrils exposed to an EGTA-relaxing solution (free of Ca2+) were adjusted to SL = 2.3 µm in order to calculate a sarcomeric passive force (Fpass), which is mostly caused by stretching titin filaments. After being Ca2+-activated with a solution containing saturating [Ca2+] (pCa 4.18), isometrically maintained myofibrils began to create force with the rate constant kact (Fig. 2 A). A brief (30 ms) release–restretch maneuver (Brenner's maneuver; Brenner, 1988) was carried out once the force had achieved its maximum and steady-state value. This caused a brief drop in force and a subsequent redevelopment of it. Thus, it is possible to estimate the total force magnitude Ftotal. When thin filaments are activated by Ca2+, this maneuver enables the determination of the active force (Fact = Ftotal− Fpass; Fig. 2 A) caused by cyclic myosin–actin crossbridges. The isometric condition is quickly disturbed during this maneuver, and the majority of crossbridges temporarily enter non-force-generating states (i.e., force drops close to zero; Fig. 2 A). Following this brief isometric–isotonic–isometric perturbation, crossbridges redistribute between non-force- and force-generating states with the rate constant ktr in a two-state model (Brenner, 1988).

Both the fapp (rate constant or probability of crossbridges entering force-generating states) and gapp (rate constant or probability of crossbridges leaving force-generating states) depend heavily on the MyHC isoform, which in turn

determines the rate constant ktr (Locher et al., 2009).). Whereas gapp is independent of [Ca2+], fapp is dependent on the thin filament state, or [Ca2+]. Consequently, ktr (= fapp + gapp) and Fact (~fapp/(fapp + gapp)) are modulated by Ca2+; Iorga et al., 2018). Myofibrils relax in two phases when Ca2+ is quickly removed. Sarcomeres maintain their small

length during the first relaxation phase, while force decays slowly and approximately linearly with the rate constant klin (Iorga et al., 2018). The second relaxation phase's force decay amplitude is significantly greater than the first phase's (Fig. 2, A and B). The second relaxation phase's rate constant, krel, represents the remaining crossbridges, leaving force-

generating states with a larger probability than gapp under a lower mechanical strain.

Figure 2: Analysis of force-related kinetic parameters of myofibrils from demembranated replated hESC-CMs. (A) Example of a force trace indicating the protocol (on top) of sarcomeric activation (+Ca2+) and relaxation (−Ca2+) and

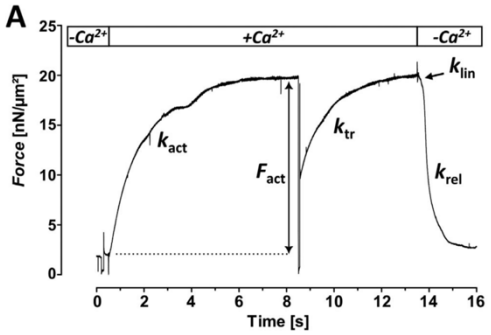

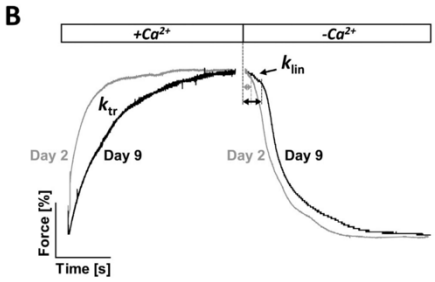

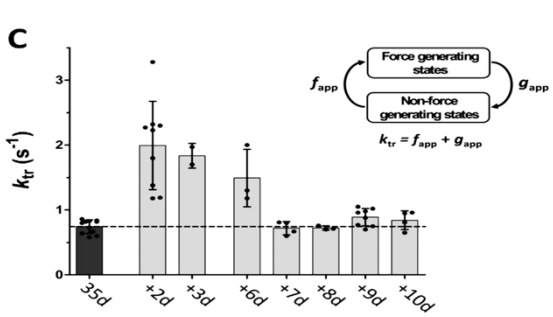

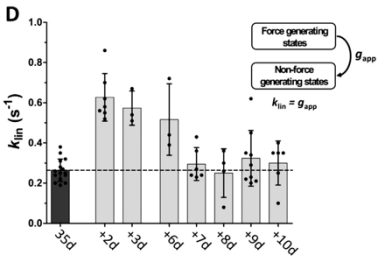

the force-related parameters: rate constant of Ca2+-induced force devel- opment (kact), amplitude of the isometric force generated by cycling crossbridges (Fact), rate constant of mechanically induced force redevelopment of Ca2+ - activated myofibrils (ktr), rate constant of the linear force decay during the first, slow phase of relaxation (klin), and the rate constant of the monoexponential force decay during the second, fast phase of relaxation (krel). (B) Force traces during force redevelopment and relaxation for myofibrils of hESC-CMs replated for 2 (grey) or 9 (black) days. Small horizontal arrows indicate the duration of the first relaxation phase (tlin) on days 2 and 9. (C and D) ktr, reflecting crossbridge cycling kinetics (C), and klin (D), reflecting crossbridges leaving force-generating states in replated hESC-CMs on indicated days, and in 35 d old non- replated hESC-CMs (data imported from Iorga et al. [2018]). Mean ± SD; n = 2–20 myofibrillar bundles obtained from 12 coverslips derived from one dif- ferentiation. Insets: Diagrams representing the two states of cycling cross-bridges. fapp: rate constant or probability of cross-bridges entering force-generating states); gapp: rate constant or probability of cross-bridges leaving force-generating states.

Examination of calcium transients within cells

As previously mentioned (Weber et al., 2020), intracellular calcium transients of single CMs were captured utilizing a dual excitation fluorescence photomultiplier system (IonOptix Corp.). Coverslips containing adherent CMs were loaded with the ratiometric indicator Fura-2 AM18 (Thermo Fisher Scientific) for 25 minutes, and then rinsed twice with DMEM for 15 minutes in order to record intracellular calcium transients of hESC-CMs cultivated for 35 days and those additionally cultivated for 1–4 days after replating. In a makeshift perfusion chamber, they were then paced by electrical stimulation at a rate of 1 Hz (25 V, 4 ms at 37 ± 0.5°C). Emission was observed at 510 nm following alternating excitation at 340 and 380 nm. Prior to computing the fluorescence ratio (340/380 nm), autofluorescence was measured from ten unloaded CMs from the same batch and subtracted from recordings. Using Ion-Wizard software (IonOptix Corp.), the time to peak, half-decay time, calcium amplitude, and calcium rise velocity were calculated.

Isolation of whole RNA

Using the peqGOLD Total RNA Kit (Peqlab; VWR Life Science; Avantor), total RNA was extracted from hESC-CMs and hiPSC-CMs that had been cultured for 37 days or replated on day 35 and cultured for two additional days in accordance with the manufacturer's instructions.

Creation of libraries, sequencing, and processing of raw data Quantification, quality assurance, and library creation

The NEBNext Ultra II Di-rectional RNA Library Prep Kit for Illumina (E7760L; New England Biolabs) was used to create stranded cDNA libraries after 70 ng of total RNA per sample was used as input for the mRNA enrichment process with the NEBNext Poly(A) mRNA Magnetic Isolation Module (E7490L; New England Biolabs). With the exception of all reactions being downscaled to two thirds of the initial volumes, every step was carried out as advised in user manual E7760 (version 1.0_02-2017; New England Biolabs). Furthermore, 1× Agencourt AMPure XP Beads (#A63881; Beckman Coulter, Inc.) were used to introduce an extra purification step at the conclusion of the normal operation. NEBNext Multiplex Oligos for Illumina—96 Unique Dual Index Primer Pairs (6440S; New England Biolabs) were used to barcode cDNA libraries using a dual indexing technique. Eleven final PCR cycles were used to amplify all produced cDNA libraries. Agilent Technologies' Bioanalyzer High Sensitivity DNA Assay (5067–4626) was used to track the fragment length distribution of each library. The Qubit dsDNA HS Assay Kit (Q32854; Thermo Fisher Scientific) was used to quantify the libraries.

Sequencing run and library denaturation:

Ten separately barcoded libraries were pooled in equal molar proportions. Consequently, 10% of the total flowcell/run capacity is made up of each examined library. In accordance with the Denature and Dilute Libraries Guide (document# 15048776 v02; Illumina), the library pool was first denatured with NaOH and then diluted to 2 pM. Using an Illumina NextSeq 550 sequencer with a High Output Flowcell for single reads (20024906; Illumina), 1.3 ml of the denatured pool was loaded. The following parameters were used for sequencing: index reads 1 and 2 with 8 bases each, and sequence reads 1 and 2 with 38 bases each. BCL to FASTQ conversion: The Illumina bcl2fastq conversion software, version v2.20.0.422, was used to convert BCL files to FASTQ files.

Processing of raw data and quality assurance

nfcore/rnaseq (version 1.4.2), a bioinformatics best-practice analysis pipeline used for RNA sequencing data at the National Genomics Infrastructure at SciLifeLab, Stockholm, Sweden, was used to process the raw data. The pipeline makes use of the bioinformatics workflow program Nextflow. It aligns the readings, preprocesses the raw data from FASTQ inputs, and thoroughly checks the output for errors. https://www.gencodegenes.org/human/release_34.html provided the genome reference and annotation data (Homo sapiens; GRCh38.p13; release 34).

Analysis of differential expression and normalisation

With DESeq2 (Galaxy Tool Version 2.11.40.2), normalisation and differential expression analysis were carried out using the default parameters, with the exception of "Output a counts table," "Turn off outliers filtering," and "Turn off independent filtering," which were all set to "True." Deposition of data You can obtain the datasets related to this work from GEO (accession no. GSE176154).

Analysis of statistics

The findings are shown as mean ± SD (for force-related parameters, calcium transient parameters, and IF analysis) or mean ± SEM (SDS-PAGE and Western blot analysis). The Mann-Whitney U-test (calcium transient parameters) or the unpaired Student's t test (force-related parameters, protein expression analysis) were used to examine differences between treated and untreated hESC-CMs or between replated and non-replated hPSC-CMs. Multiple differentiations of hPSC-CMs were taken into consideration in experiments pertaining to Figures 3 and 4 C using a nested t-test. A difference was considered significant if it was $P < 0.05$ (p), $P < 0.01$ (pp), or $P < 0.001$ (ppp). To conduct statistical studies, GraphPad Prism 9.5.1 was utilized.

RESULTS

Changes in replated hESC-CMs' contractile function

We measured the functional parameters of sub-cellular myofibrils from chemically demembranated hESC-CMs in order to examine the possible impact of detachment from the stiff substrate and subsequent replating of long-term plated hESC-CM on contractile function. The force-related kinetics of isometrically maintained myofibrils were assessed from days 2–10 following replating of hESC-CMs that had been enzymatically separated from and subsequently replated on laminin-coated coverslips (Fig. 2, A–D; see Table 1). To reduce the possible variations caused by Ca2+-regulation at intermediate [Ca2+] between the myofibrils of replated and non-replated hESC-CMs, experiments were conducted at saturating [Ca2+]. When compared to control, non-replated hESC-CMs, Ca2+-activated, replated hESC-CMs produced a lower maximum isometric force (Fact) normalised to the myofibrillar bundle's cross-section (Table 1). When compared to non-replated, exclusively β-MyHC-expressing hESC-CMs, the rate constant of force development kact was considerably higher on day 2 when completely Ca2+-activated (pCa 4.18) (Iorga et al., 2018; Table 1). When compared to non-replated, exclusively β-MyHC-expressing hESC-CMs (Iorga et al., 2018), the rate constant of force development (ktr) and the rate constant of slow force decay (klin) during the first relaxation phase after Ca2+ removal were also significantly increased on day 2 (Fig. 2, C and D; and Table 1). This was after a quick release–restretch maneuver. On day two, the ktr value of replated hESC-CMs (2.01 ± 0.64 s−1) was close to the ktr of hESC-CMs that solely expressed α-MyHC (2.44 ± 0.30 s−1; Weber et al., 2016). Myofibrils from replated hESC-CMs on days 2–6 had a somewhat shorter duration (smaller tlin) for the initial relaxation phase than myofibrils from non-replated cells or on days 7–10 (Fig. 2 B and Table 1). For myofibrils of every cell under investigation, the mean values of the rate constant krel were comparable (Table 1). In the second week following replating, the kinetic parameter changes from days 2–6 were reversed (Fig. 2, C and D; and Table 1). When combined, the data show that myo-fibrillar force-related kinetic parameters representing crossbridge cycling in replated hESC-CMs' sarcomeres changed for up to 6 days following replating, but that these changes were entirely reversed in the second week (Table 1). The rate constants (or probabilities) of crossbridges entering (fapp) and exiting (gapp) force-generating states can be directly determined using ktr and klin, in accordance with the two-state crossbridge model (Brenner, 1988; Iorga et al., 2018) (Fig. 2, C and D). Fapp and gapp considerably increased in hESC-CMs replated for 2 days when compared to non-replated cells that were 35 days old (Table 2), but the did not significantly change in hESC-CMs replated for 9 days (Table 2), suggesting that the changes that were observed were reversible.

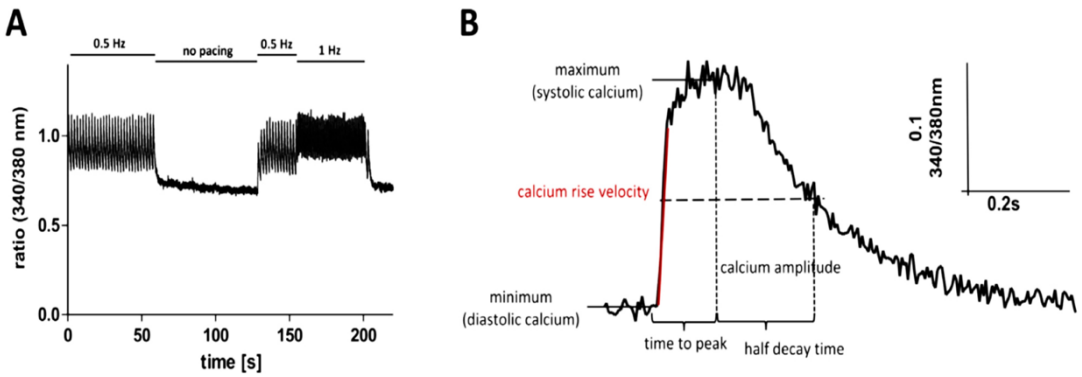

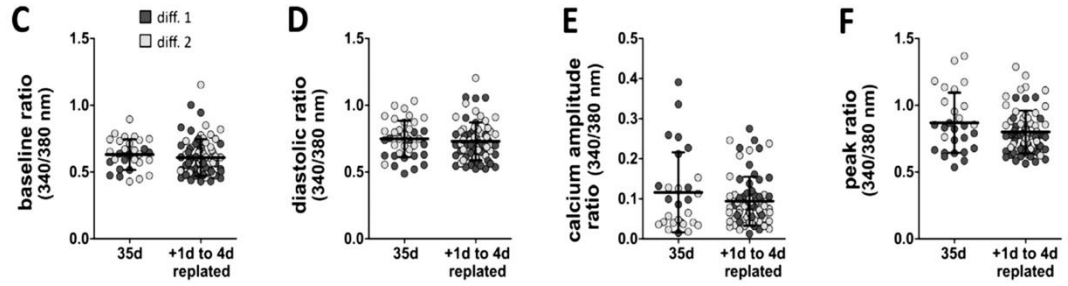

Figure 3. Calcium transients from hESC-CMs replated for 1 to 4 d from day 35 onward without electrical pacing and then paced with 1 Hz.

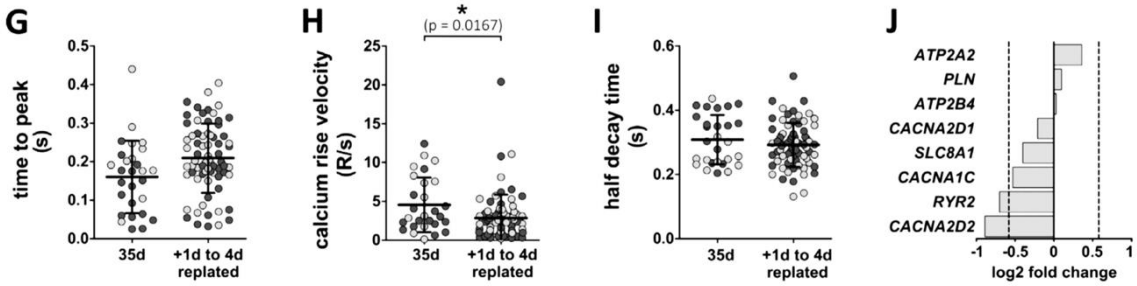

Representative electrical stimulation protocol. Stimulation with 0.5 Hz for 1 min, followed by a stimulation break for registration of basal ratio (basal calcium). The basal ratio was measured at the end of the break where ratio reached a stable phase. Then, the frequency was increased from 0.5 to 1 Hz for ~1 min. Calcium transients were analysed during 1 Hz stimulation. (B) Representative averaged calcium transient with analysed parameters of minimum (diastolic), maximum (systolic, peak ratio) 340/380 nm ratios, calcium amplitude (difference between maximum and minimum 340/380 nm ratios), time to peak, half decay time, and maximum calcium rise velocity (red). Parameters were calculated after fitting the averaged calcium transients using IonWizard software. (C–I) Baseline calcium level (C) without electrical stimulus (baseline ratio 340/380 nm), (D) diastolic (minimum) calcium level (diastolic ratio 340/380 nm), (E) calcium amplitude (ratio 340/380 nm), (F) peak ratio (peak ratio 340/380 nm, maximum calcium level), (G) time to peak (in s), (H) calcium rise velocity (R/s; R: ratio 340/380 nm), and (I) half-decay time of calcium transients (in s). Calcium transients were determined under electrical stimulation with 1 Hz using the ratiometric calcium indicator Fura-2 and compared with non-replated hESC-CMs. Ratio: emission at 510 nm measured after alternating excitation at 340 nm/380 nm. Mean ± SD; n = 28–71 cells from 5–20 individual coverslips derived from two differentiations. Cells are colored according to the hESC-CM differentiation they were derived from (dark grey: differentiation no. 1; light grey: differentiation no. 2). *, $P < 0.05$. (J) hESC-CMs grown for 35 d on laminin coated glass coverslips were detached, replated, cultivated for two additional days, and compared with 37-d-old non-replated cells; n = 3. mRNA expression for indicated genes of calcium handling was analysed by RNA-seq. Data are presented as log2 fold change. The dashed line at ±0.585 indicates a ±1.5-fold change.

Calcium transient changes in replated hESC-CMs

Additionally, we used the ratiometric calcium indicator Fura-2 to quantify intracellular calcium transients of intact, single hESC-CMs upon loading (Fig. 3, A and B). Without electrical stimulation, there was no difference in the baseline

calcium level between long-plated and replated hESC-CMs (Fig. 3 C). When hESC-CMs were electrically stimulated at a frequency of 1 Hz, their minimum (diastolic) calcium level, calcium amplitude, and highest (systolic, peak) calcium level (peak ratio) remained unchanged when compared to cells that were not replated (Fig. 3, D–F). The maximum calcium increase velocity was slower in replated hESC-CMs than in non-replated hESC-CMs (Fig. 3, G, and H), but the time to peak was not substantially changed. Calcium transients' half decay duration remained unchanged (Fig. 3 I). When comparing hESC-CMs replated for 2 days to 37-day-old controls, RNA-sequencing (RNA-Seq) revealed lower mRNA expression levels of the genes encoding for calcium-handling proteins, CACNA1C, CACNA2D2, and RYR2 (Fig. 3 J). This is in line with the slower kinetics of calcium transients in replated CMs.

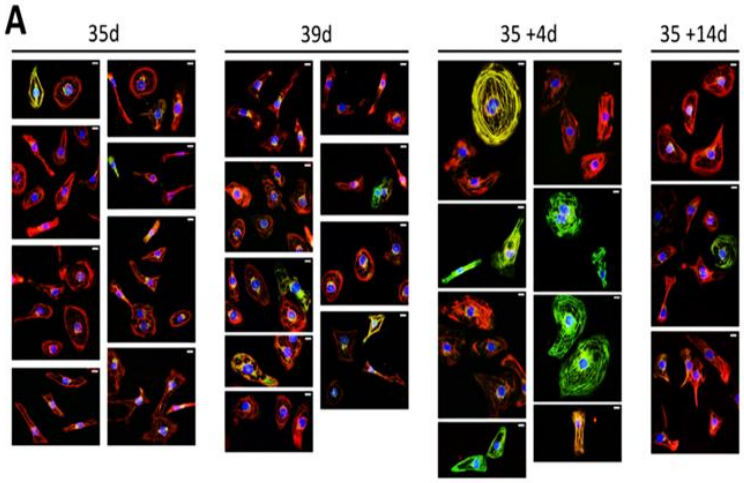

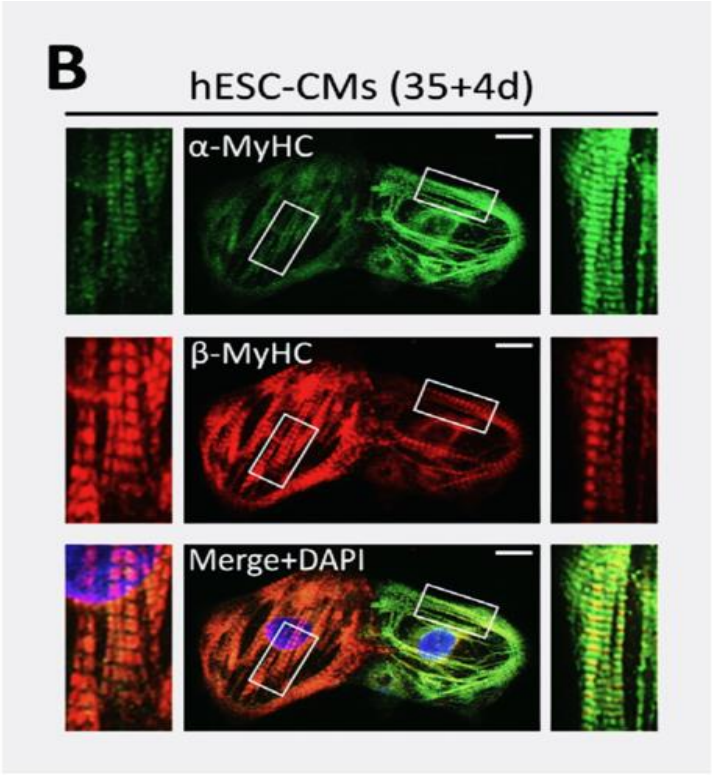

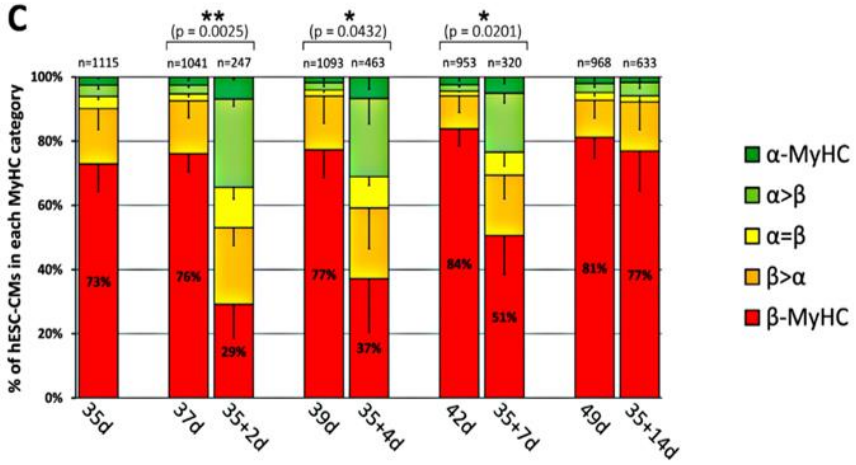
C
** (p = 0.0025)
* (p = 0.0432)
* (p = 0.0201)
n=1115
n=1041 n=247
n=1093 n=463
n=953 n=320
n=968 n=633
% of hESC-CMs in each MyHC category
100%
80%
60%
40%
20%
0%
73%
76%
29%
77%
37%
84%
51%
81%
77%
35d
37d
35+2d
39d
35+4d
42d
35+7d
49d
35+14d
α-MyHC
α>β
α=β
β>α
β-MyHC

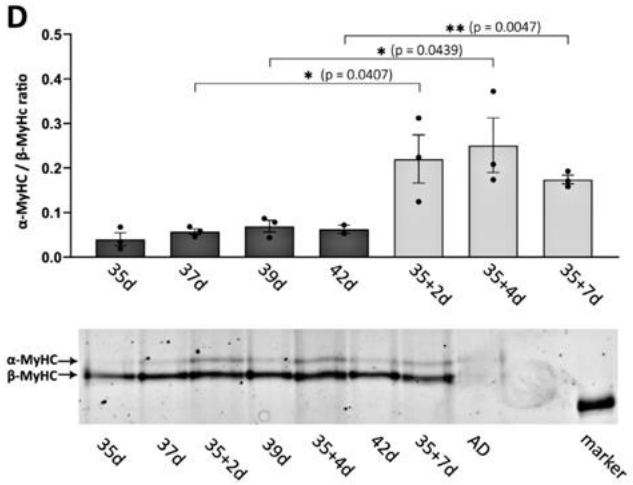
D
** (p = 0.0047)
* (p = 0.0439)
* (p = 0.0407)
α-MyHC / β-MyHc ratio
0.5
0.4
0.3
0.2
0.1
0.0
35d
37d
39d
42d
35+2d
35+4d
35+7d
α-MyHC
β-MyHC
35d
37d
35+2d
39d
35+4d
42d
35+7d
AD
marker

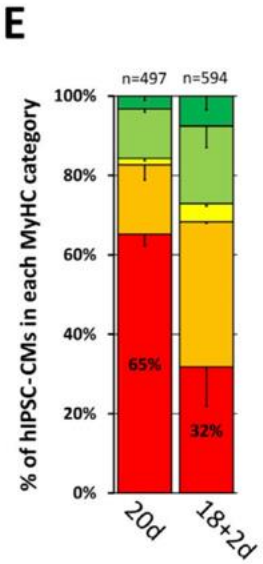
E
n=497
n=594
% of hIPSC-CMs in each MyHC category
100%
80%
60%
40%
20%
0%
65%
32%
20d
18+2d

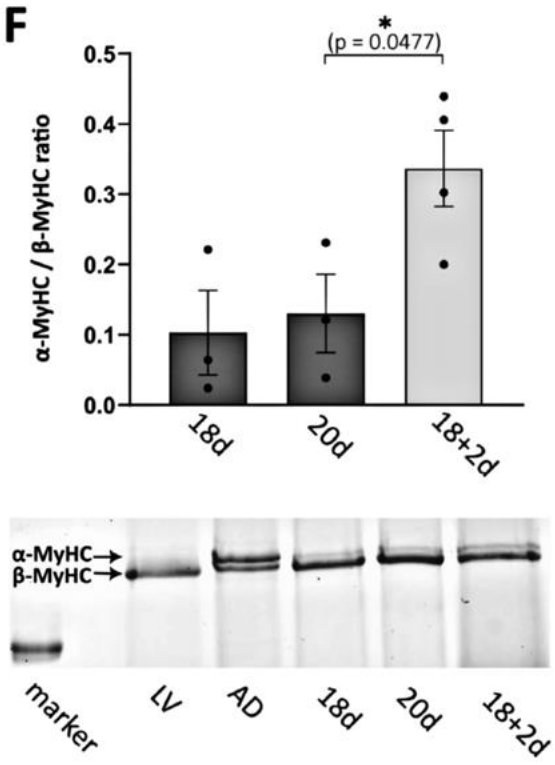

Figure 4 : Analysis of myosin isoform expression in replated hPSC-CMs. hESC-CMs or hiPSC-CMs were cultivated for indicated days on laminin-coated glass coverslips or replated on day 35 or day 18, respectively, and further cultivated for indicated days. (A) Myosin isoform expression was analyzed in hESC- CMs by single-cell immunofluorescence (IF) using specific antibodies against α- (green) and β-MyHC (red). Nuclei were stained with DAPI (blue). Scale bars: 10 μm. (B) Single-cell IF analysis showing replated hESC-CMs from 35 + 4 d with mixed α- and β-MyHC expression with insets (white squares) demonstrating a detailed view of sarcomeric staining as relevant for classification (see below). Scale bars: 10 μm. (C) Single-cell IF analysis of myosin expression in hESC-CMs. The fractions of cells in the different categories (see Materials and methods) are shown as the percentage of the total number of cells analyzed (n, set to 100%) for each time point. Mean ± SD; indicated number of cells (n) were obtained from six individual coverslips derived from three differentiations; P values: exclusively β-MyHC expressing cells. (D) MyHC isoforms were separated by SDS-PAGE and the ratio of α-MyHC/β-MyHC expression in hESC-CMs was determined densitometrically.

Mean ± SEM; n = 3 individual coverslips from three differentiations. Representative SDS-PAGE gel with samples from human right atrium (AD) as indicated; molecular weight marker: 200 kD. (E) Myosin isoform expression was analyzed in hiPSC-CMs by single-cell IF using specific antibodies against α- and β-MyHC. The fractions of cells in the different categories (see Materials and methods) are shown as a percentage of the total number of cells analyzed (n, set to 100%) for each time point. Mean; two coverslips derived from one differentiation. (F) MyHC isoforms were separated by SDS-PAGE and the ratio of α-MyHC/β-MyHC expression in hiPSC-CMs was determined densitometrically. Mean ± SEM; n = 3 or 4 individual coverslips from one differentiation. Representative SDS-PAGE gel, with samples from the human right atrium (AD) and left ventricle (LV) as indicated; molecular weight marker: 200 kD. Source data are available for this figure: SourceData F4.

Enhanced α-MyHC expression in replated hESC and hiPSC CMs

The rate constants of force-generating cross-bridge states that we found to be modified in replated hESC-CMs (Table 2) rely on MyHC isoform expression (Locher et al., 2009). Therefore, we used hESC-CMs that had been removed and replated on day 35 of culture to undertake single-cell immunofluorescence (IF) analysis in order to evaluate the expression of α-/β-MyHC isoforms. Sarcomeric formations were difficult to identify one day after replating (data not shown), but they were visible on day two. On days 2, 4, and 7, replated hESC-CMs exhibited a strong rise in exclusively α-MyHC and mixed α/β-MyHC expression, as demonstrated by single-cell IF analysis (Fig. 4, A–C). This resulted in a significant increase in the heterogeneity of MyHC isoform expression across CMs in comparison to non-replated controls. It's interesting to note that after 14 days, the amount of replated hESC-CMs that solely expressed β-MyHC rose once more and was on par with non-replated controls. SDS-PAGE examination verified that replated hESC-CMs expressed more α-MyHC than non-replated CMs (Fig. 4 D and Table 3). A similar change from predominantly β-MyHC-expressing cells to more exclusive α-MyHC and heterogeneous α-/β-MyHC expression was also brought about by

replating hiPSC-CMs (Fig. 4, E and F; and Table 3), suggesting that the effects seen are not limited to CMs produced from hESCs. Additionally, hESC-CMs that were detached and replated on days 42, 45, 48, and 55 following prolonged long-term cultivation on a stiff matrix showed higher expression of exclusively α-MyHC and mixed α/β-MyHC compared to day 34 (Fig. 5, A–E). After two weeks, the predominance of hESC-CMs that expressed exclusively β-MyHC showed some variation. The mRNA expression profile of genes encoding sarcomeric proteins that have been demonstrated to impact myofibrillar contractile function was also examined using RNA-Seq (Iorga et al., 2018).

MYH6 mRNA expression of hESC-CMs replated for 2 d was profoundly up-regulated (fold change 3.52; Fig. 5 F and Table 4) compared with non-replated cells, while the mRNA expression of MYH7 (fold change−1.59; Fig. 5 F and Table 4) was less affected, resulting in a nearly equal level of MYH6 and MYH7 mRNA in replated hESC-CMs. Additionally, there was less of an impact on the expression of genes corresponding to troponins and myosin light chain isoforms (Fig. 5 F). In conclusion, MyHC isoform expression study showed that long-term plated hPSC-CMs' separation and subsequent replating caused a sharp rise in α-MyHC expression, which may account for the observed variations in kinetic parameters related to myofibrillar force.

Force-related parameters	35 d	+2 d	+3 d	+6 d	+7 d	+8 d	+9 d	+10 d
F_{act} (kPa)	42 ± 10	32 ± 11	26 ± 11	24 ± 2[a]	22 ± 9[a]	18 ± 6[a]	25 ± 10[a]	22 ± 10[a]
k_{act} (s^{-1})	0.66 ± 0.14	1.56 ± 0.33[a]	1.64 ± 0.48	1.26 ± 0.27	0.75 ± 0.12	0.64 ± 0.02	0.69 ± 0.05	0.64 ± 0.02
k_{tr} (s^{-1})	0.75 ± 0.10	2.01 ± 0.64[a]	1.84 ± 0.19	1.49 ± 0.44	0.72 ± 0.10	0.72 ± 0.03	0.88 ± 0.12	0.84 ± 0.15
k_{lin} (s^{-1})	0.26 ± 0.06	0.64 ± 0.11[a]	0.57 ± 0.09[a]	0.52 ± 0.18	0.30 ± 0.08	0.25 ± 0.12	0.33 ± 0.13	0.30 ± 0.11
t_{lin} (ms)	197 ± 60	165 ± 61	134 ± 45	156 ± 51	191 ± 77	195 ± 92	199 ± 42	212 ± 46
k_{rel} (s^{-1})	4.62 ± 0.60	4.69 ± 2.15	3.93 ± 0.04	4.80 ± 0.79	4.02 ± 1.16	4.10 ± 0.91	4.33 ± 2.28	4.43 ± 0.96

Table 1: Force-related steady-state and kinetic parameters of myofibrils from replated hESC-CMs

Force-related steady-state (Fact) and kinetic parameters (kact, ktr, klin, tlin, krel) of myofibrils from hESC-CMs replated for indicated days, and of non-replated (35 d) hESC-CMs (data imported from Iorga et al. [2018]). Data for most relevant cross-bridge-related parameters ktr and klin are also shown in Fig. 2, C and D. aSignificance level at least $P < 0.05$ or smaller.

Cross-bridge related parameters	Replated hESC-CMs		Non-replated
	2 d	9 d	35 d hESC-CMs
f_{app}	1.32 ± 0.75**	0.56 ± 0.16[ns]	0.47 ± 0.11
g_{app}	0.64 ± 0.11**	0.33 ± 0.13[ns]	0.26 ± 0.06

Table 2 : Kinetic parameters reflecting probabilities of cross-bridges to enter and leave force-generating states of replated hESC-CMs

Kinetic parameters reflecting probabilities of cross-bridges to enter (fapp) and leave (gapp) force-generating states of replated cells on indicated days, and of non-replated 35 d hESC-CMs with predominant exclusive β-MyHC expression (data imported from Iorga et al. [2018]). Data were calculated as indicated in Fig. 2, C and D. Mean ± SD; **, $P < 0.01$; ns, not significant, $P > 0.05$).

Changes in mechanosensation/transduction are indicated by gene enrichment analysis.

The functional enrichment analysis web tool WebGestalt (WEB-based Gene SeT AnaLysis Toolkit; Liao et al., 2019) was used to perform gene enrichment analysis based on RNA-Seq data of hESC-CMs replated for 2 days after 35 days of growth as compared with 37 days old non-replated controls. Significantly enhanced biological process categories linked

to ECM and cell adhesion (Fig. 6 A) and muscle growth and function (Fig. 6 B) were revealed by gene ontology (GO) analysis of up-regulated genes (fold change cutoff 1.5). This highlights how changes in matrix stiffness affect how cardiomyocytes interact with a rearranged extracellular matrix and how they function at the gene expression level. Accordingly, pathways involved in mechanosensation/transduction in the cardiomyocyte response to mechanical stretch were significantly enriched by Ingenuity Pathway Analysis (IPA; Qiagen) (Dostal et al., 2014; Sashima and Izumo, 1997), primarily integrin- and, to a lesser extent, G-protein-associated pathways, with only a small number of calcium-associated pathways being enriched (Fig. 6 C). Together, these categories enriched in GO analysis and IPA are linked to cell interaction and ECM organization, as well as mechanosensation/transduction with an emphasis on integrin-associated signaling, in accordance with a change in matrix stiffness during dissociation and replating of the hESC-CMs.

FAK inhibition lowers the expression of β-MyHC.

We examined the expression and phosphorylation levels of FAK and its downstream mediator ERK1/2 in hESC-CMs in order to better explore the potential influence of integrin-dependent signaling on the expression of MyHC-isoforms. FAK and ERK1/2 activation in hESC-CMs on days 7–35 was demonstrated by Western blot analysis, which also showed expression and phosphorylation (Fig. 7 A). The ratio of phospho-ERK1/2/total ERK1/2 was unaffected by FAK inhibitor 14 (5 μM) inhibiting FAK, suggesting that ERK1/2-phosphorylation in 35-d-old hESC-CMs is largely independent of FAK activation (Fig. 7 B). In hESC-CMs treated for 2 or 4 days with 5 μM FAK inhibitor 14, IF analysis showed a decrease in solely β-MyHC expression; however, 10 μM U0126, an inhibitor of ERK1/2 direct upstream kinase MEK1/2, had no discernible effect (Fig. 7 C). According to the data, FAK favourably regulates β-MyHC expression, whereas MEK1/2–ERK1/2 signaling has no effect. Only a small percentage of 35-d-old hESC-CMs grown on laminin-coated glass coverslips express the ventricular MLC isoform 2v exclusively, in contrast to β-MyHC expression (see Fig. 4). This suggests that rigid matrix has a different influence on the expression of ventricular MyHC and MLC2 isoforms (Fig. 7 D). On a softer matrix, Matrigel-coated polydimethylsiloxane (PDMS), the percentage of MLC2v that expressed hESC-CMs was raised, both exclusively and among all MLC2v.

DISCUSSION

In hESC-CMs that were long-term cultivated on a rigid matrix, detached, and then replated, the work presented shows a rapid increase in α-MyHC expression and its impact on calcium transients and myofibrillar contractile activity. The observed alterations in the mix of MyHC isoforms that impact cross-bridge turnover kinetics are probably reflected in the notable variations in rate constants between replated and non-replated cells (Locher et al., 2009). According to the data, cross-bridge kinetics in replated hESC-CMs were faster in the first few days (up to one week) after replating. This was probably caused by increased ATPase activity associated with re-expression of the α-MyHC isoform. Replated cells may have a higher tension cost, a possibility supported by a lower isometric force, as indicated by the higher gapp values observed in replated hESC-CMs. These values also reflect an increased risk of cross-bridges entering non-force-generating states. As a result, α-MyHC re-expression may affect cellular energetics at the sarcomeric level.

	hESC-CMs									hiPSC-CMs	
α-MyHC	**35 d**	**37 d**	**35 + 2 d**	**39 d**	**35 + 4 d**	**42 d**	**35 + 7 d**	**49 d**	**35 + 14 d**	**20 d**	**18 + 2 d**
Mean (%)	3.86	5.46	17.73	6.48	19.72	5.92	14.83	8.61	5.32	11.12	24.82
± SD (%)	2.27	0.98	6.38	2.02	6.52	1.15	1.26	6.37	1.93	7.51	6.26

Table 3 : Relative α-MyHC protein expression in replated hPSC-CMs

α-MyHC protein expression relative to total MyHC isoform protein expression (in percent) of replated and non-replated hESC- and hiPSC-CMs on indicated days. MyHC isoforms were separated by SDS-PAGE and MyHC isoform expression was determined densitometrically (see Fig. 4, D and F). Mean, hESC-CMs: n = 3 culture dishes from three differentiations; hiPSC-CMs: n = 3 or 4 culture dishes from one differentiation.

Figure 5: IF analysis of myosin isoform expression in single hESC-CMs replated at different times.

(A–E) hESC-CMs grown for (A) 34, (B) 42, (C) 45, (D) 48, and (E) 55 d on laminin-coated glass coverslips were detached, replated on laminin-coated glass coverslips, grown for the indicated number of days (+d), and compared with

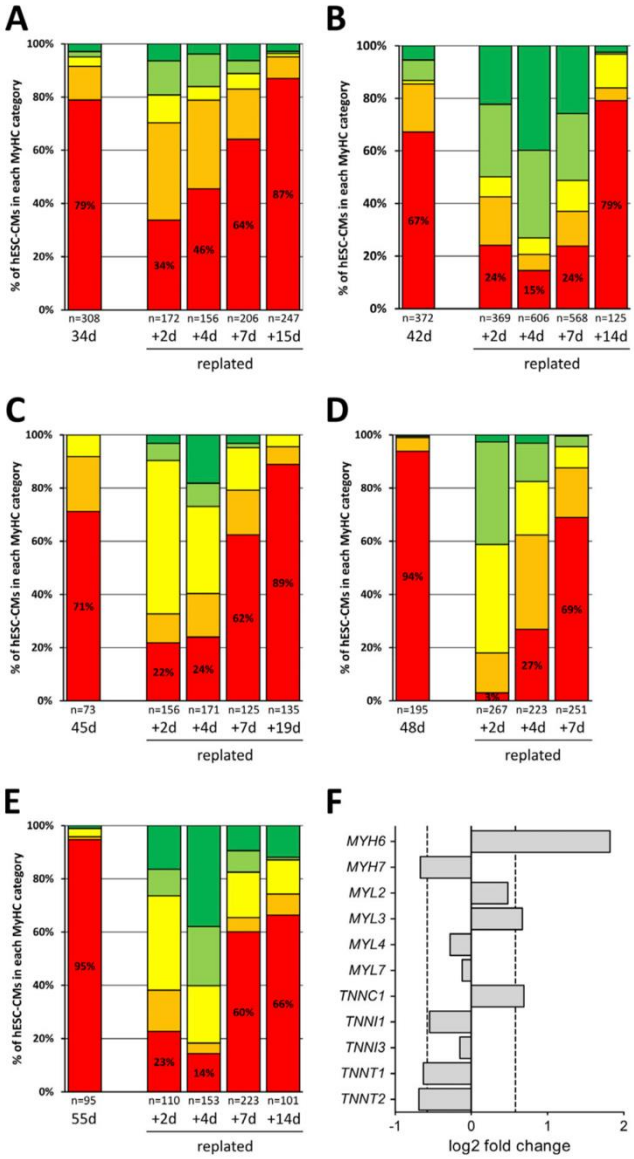

non-replated controls (d). Myosin isoform expression was analyzed by single-cell IF using specific antibodies against α- and β-MyHC. The fractions of cells in the different categories are shown as a percentage of the total number of cells analyzed (n, set to 100%) for each time point
(see Materials and methods). One coverslip from one differentiation each.(F) Changes in sarcomeric gene expression (log2 fold change) of hESC-CMs after replating compared with 37 d old non-replated controls. hESC-CMs grown for 35 d on laminin-coated glass coverslips were detached, replated on laminin- coated glass coverslips and cultivated for two more days. mRNA expression was analyzed using RNA-Seq data. Changes in mRNA expression of indicated myosin heavy chain (MYH), myosin light chain (MYL), and troponin (TNN) isoform genes are presented as log2 fold change. The dashed line at ±0.585 indicates a ±1.5- fold change; n = 3 culture dishes from three differentiations.

	Base mean			
Gene name	**37 d**	**35 + 2 d**	**log2(FC)**	**P-adj**
MYH6	20,165	107,324	1.82	4.52×10^{-7}
MYH7	201,052	106,418	−0.67	3.49×10^{-1}

Table 4 : MYH isoform mRNA expression in replated hESC-CMs

MYH6 and MYH7 mRNA base means in replated (35 + 2 d) vs. non-replated control (37 d) hESC-CMs derived from RNA-Seq. Base means, log2 fold change (log2(FC)), and adjusted P value (P-adj) from n = 3 culture dishes from three differentiations. Normalisation and differential expression analysis was performed with DESeq2.

When compared to non-replated long-term cultivated hESC-CMs, changes in force-related kinetic parameters in replated hESC-CMs expressing significant amounts of α-MyHC are consistent with reports suggesting that the expression of the MyHC isoform is the primary determinant of contractility and heart power output (Herron and McDonald, 2002; Palmiter et al., 1999). It has been demonstrated that the expression of the MyHC isoforms controls the amplitude and velocity of sarcomere shortening, independent of Ca2+ handling (Herron et al., 2007, 2010). It's interesting to note that the transition from predominant β-MyHC to mixed α-/β-MyHC expression appears to be primarily caused by much higher MYH6 expression and very marginally by MYH7 down-regulation. Within 1-2 weeks following transplantation, this relatively preserved MYH7 mRNA expression may aid in the retransition to cells that mostly express β-MyHC. Changes in myofibrillar force-related kinetic characteristics may be explained by a change in the expression of the MyHC isoform protein, however this does not always explain the decline in force production following replating. Accordingly, the duty ratio (fapp/fapp + gapp), which is thought to kinetically modify the steady state force level, remained largely unchanged for both non-replated (35 d: 0.64 ± 0.08) and replated (35 + 2 d: 0.67 ± 0.15; 35 + 9 d: 0.63 ± 0.14), CMs. Thus, the force drop may be caused by additional causes, such as substantial sarcomeric remodeling. Additionally, the expression of various isoforms of other sarcomeric proteins also affects the functional properties of CMs (Iorga et al., 2018).
Remarkably, alterations in MYL and TNN isoforms' mRNA expression that were connected to replating were less significant than those in MYH6 isoform expression. However, neither the Z-disk components nor the protein expression of MLCs (particularly ventricular, see Fig. 5 F) that could influence isometric force following replating are excluded by our data. The observed changes in protein and gene expression, and consequently function, were probably caused by changes in ECM stiffness, i.e., a decreased mechanical load or stress following the detachment of the long-term plated hESC-CMs. Changes in mechanosensation/transduction-related gene expression, particularly integrin-related signaling, as shown by GO and IPA analysis based on RNA-Seq data, corroborate this result. GO analysis revealed a number of enriched categories pertaining to cell contact and ECM organization, most likely reflecting effects brought on by variations in matrix rigidity. In heart development and growth, it has been demonstrated that substrate stiffness influences the mechanosensing and signaling pathways of CMs (Gaetani et al., 2020; Munch and Abdelilah-Seyfried, 2021). The structural foundation of mechanotransduction is formed by the costameres, a complex network of proteins that link the sarcomeres to the extracellular matrix (Harvey and Leinwand, 2011). Numerous mechano-sensation/-transduction pathways associated with integrins, G-protein-coupled receptors, and calcium channels have been demonstrated to impact cardiomyocyte function (Dostal et al., 2014). Integrins are able to detect changes in the stiffness of the extracellular matrix (ECM) and communicate these changes through integrin-dependent pathways, such as FAK (Pentassuglia and Sawyer, 2013). It has been shown that concentric hypertrophy with elevated MYH7 mRNA expression is caused by FAK over-expression in mice (Clemente et al., 2012). The intercalates disc may also experience integrin-dependent mechanosensation (Pruna and Ehler, 2020).

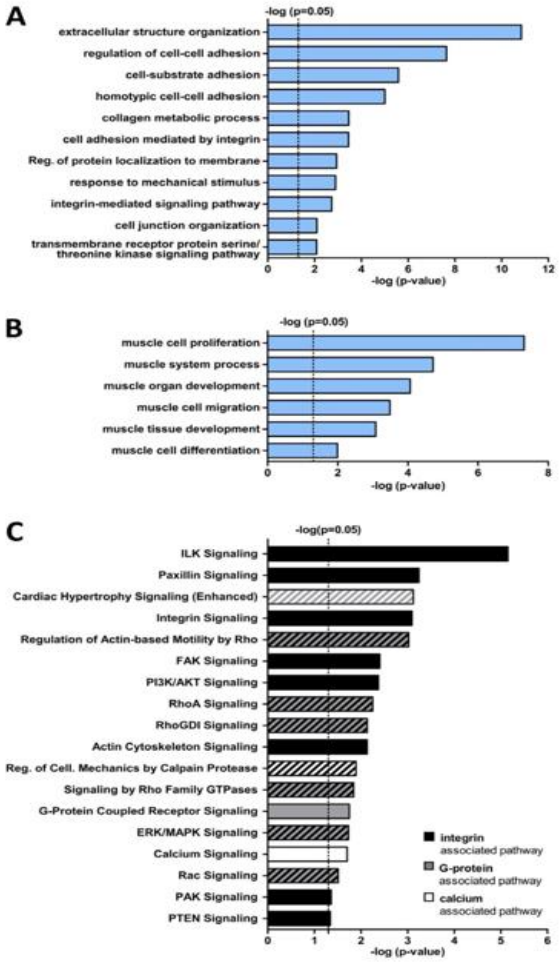

Figure 6 : Gene enrichment analysis based on RNA-seq data of replated (35 + 2 d) vs. non-replated control (37 d) hESC-CMs. hESC-CMs grown for 35 d on laminin-coated glass coverslips were detached, replated on laminin-coated glass coverslips, and grown for an additional 2 d. Gene expression was compared with 37-d-old controls (fold change cutoff 1.5; n = 3). (A and B) Enriched biological process categories related to (A) ECM and cell adhesion, and (B) muscle development and function as demon-
strated by GO analysis of up-regulated genes using the functional enrichment analysis web tool WebGestalt. Sorted by−log P value ranking (Fisher's exact test) with $P < 0.05$ set as the threshold. (C) IPA (Qiagen) revealed canonical pathways involved in mechanosensation/-transduction. Integrin-, G-protein- and calcium-associated pathways are indicated with a threshold of $P < 0.05$. Significance values (P value of overlap) for canonical pathways are calculated by the right-tailed Fisher's exact test; n = 3 culture dishes from three differentiations. Combinations of black-, white-, or gray-
striped bars refer to the involvement of signaling in two of the pathway categories as indicated by the legend.

Additionally, sarcomere structures can sense changes in mechanical load, and the protein phosphatase calcineurin is a significant downstream mediator that can influence MYH7 expression, at least in hypotrophic conditions (Linke and Kn¨ oll, 2010; Lyon et al., 2015). Pharmacological interference tests with replated hESC-CMs (not shown) and data from IPA canonical pathway analysis indicate that integrin, rather than calcium signaling, is mostly responsible for replating-related alterations in gene expression. We could show that integrin downstream mediator FAK is involved in the control of β-MyHC expression in agreement with GO and IPA analysis, highlighting the importance of mechano-sensation/-transduction for matrix-induced alterations. It is interesting to note that, in contrast to laminin-coated glass coverslips, a greater dose (10 μM) of the FAK inhibitor 14 was demonstrated to reduce β-MyHC expression in hiPSC-CMs grown on Matrigel-coated PDMS (Herron et al., 2016), a softer matrix. ERK1/2 MAPK did not mediate the impact of FAK on MyHC expression in hESC-CMs. Therefore, it is still unclear exactly how integrin signaling mediates the effects of replating generally and on MYH/MyHC isoform production in particular. HiPSC-CMs cultivated in engineered heart tissue (EHT) were exposed to elevated mechanical load by applying increased after-load. Molecular responses from hiPSC-CMs have been demonstrated (Leonard et al., 2018).

MYH7/MYH6 mRNA and β-/α-MyHC protein ratios rose along with the expression of other cardiac-specific sarcomeric genes as a result of increasing after load, which aided in maturation. The expression of the mechanosensitive muscle-specific chaperone melusin (ITGB1BP2) also increased at the highest after-load conditions. These results show that mechanical strain can also alter sarcomeric gene expression in 3-D cultures, most likely by mechanosensation/transduction. The relative abundance of α-MyHC in hiPSC-CMs increased with greater shortening or contractile work, according to a noteworthy investigation with EHTs that found a high link between the MyHC isoform ratio and shortening velocity (Ng et al., 2021). In summary, the data show that mechanosensation/transduction changes when the matrix stiffness varies during the process of removing and re-introducing hPSC-CMs for functional assessments. The observed quick transition from predominant β-MyHC-expression to up-regulated α-MyHC-expression, together with concomitant changes in calcium transients and contractile performance, is thought to be caused by altered mechanosensation/transduction involving integrin-related signaling. To effectively undo the induced alterations in MyHC isoform expression and contractile function, culture must be continued for at least one week following replating. It is important to consider these modifications when hPSC-CMs are separated and replated, especially for further in vitro

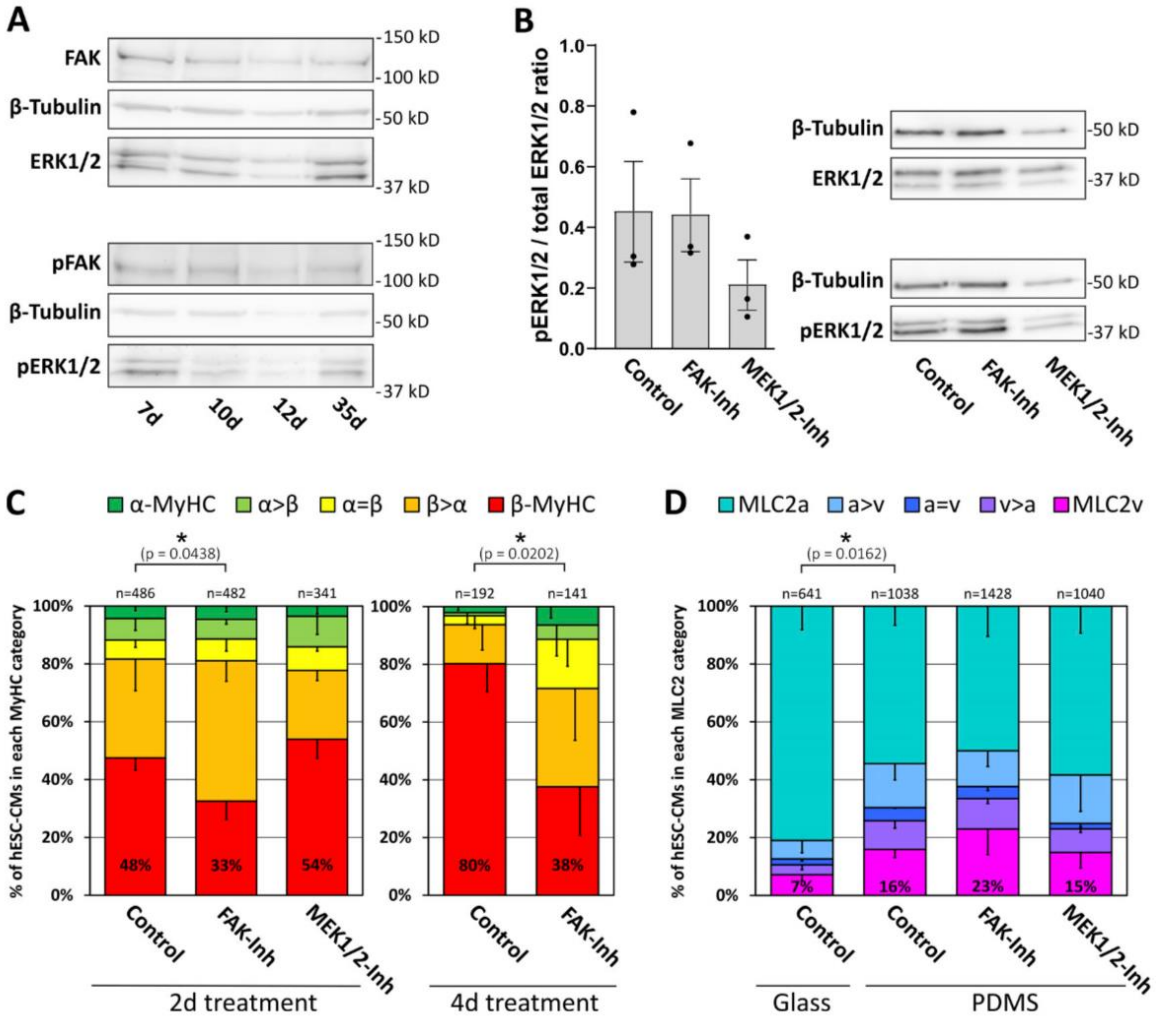

tests.

Figure 7. β-MyHC expression is reduced by inhibition of FAK.

CMs grown for indicated days on laminin-coated glass coverslips. Representative blot, with β-tubulin serving as a loading control. (B) Western blot analysis of ERK1/2-MAPK phosphorylation in 35 d hESC-CMs grown on Matrigel-coated PDMS treated with or without 5 µM FAK-inhibitor 14 (FAK-Inh) or 10 µM MEK1/2 inhibitor U0126 (MEK1/2-Inh) for 2 d. The ratio of phospho/total ERK1/2-MAPK expression was determined densitometrically. Mean ± SEM; n = 3 individual coverslips from one differentiation. Representative blot, with β-tubulin serving as a loading control. (C) Myosin isoform expression was analyzed by single-cell IF using specific antibodies against α-MyHC and β-MyHC in hESC-CMs grown on laminin-coated glass coverslips treated with or without 5 µM FAK-inhibitor 14 (FAK-Inh) or 10 µM MEK1/2 inhibitor U0126 (MEK1/2-Inh) from day 7 on for 2 or 4 d. The fractions of cells in the different indicated

categories (see Materials and methods) are shown as a percentage of the total number of cells analyzed (n, set to 100%, from three coverslips derived from one differentiation; P values: exclusively β-MyHC expressing cells. (D) hESC-CMs were grown for 35 d on laminin-coated glass coverslips or on Matrigel-coated PDMS and treated with or without 5 µM FAK-inhibitor 14 (FAK-Inh) or 10 µM MEK1/2 inhibitor U0126 (MEK1/2-Inh) for 2 d as indicated. MLC2 isoform expression was analyzed by single- cell IF using specific antibodies against MLC2v and MLC2a. The fractions of cells in the different categories (see Materials and methods) are shown as a percentage of the total number of cells analyzed (n, set to 100%, from three coverslips derived from one differentiation; P values: exclusively MLC2v expressing cells). Source data are available for this figure: SourceData F7.

REFERENCES

1. Brenner, B. 1988. Effect of Ca2+ on cross-bridge turnover kinetics in skinned single rabbit psoas fibers: Implications for regulation of muscle contraction. Proc. Natl. Acad. Sci. USA. 85:3265–3269 https://doi.org/10.1073/pnas.85.9.3265
2. Castillo, E.A., K.V. Lane, and B.L. Pruitt. 2020. Micromechanobiology: Focusing on the cardiac cell-substrate interface. Annu. Rev. Biomed. Eng. 22:257–284. https://doi.org/10.1146/annurev-bioeng-092019-034950
3. Chatterjee, S., T. Hofer, A. Costa, D. Lu, S. Batkai, S.K. Gupta, E. Bolesani, R. Zweigerdt, D. Megias, K. Streckfuss-B¨ omeke, et al. 2021. Telomerase therapy attenuates cardiotoxic effects of doxorubicin. Mol. Ther. 29: 1395–1410. https://doi.org/10.1016/j.ymthe.2020.12.035
4. Clemente, C.F., J. Xavier-Neto, A.P. Dalla Costa, S.R. Consonni, J.E. Antunes, S.A. Rocco, M.B. Pereira, C.C. Judice, B. Strauss, P.P. Joazeiro, et al. 2012. Focal adhesion kinase governs cardiac concentric hypertrophic growth by activating the AKT and mTOR pathways. J. Mol. Cell. Cardiol. 52: 493–501. https://doi.org/10.1016/j.yjmcc.2011.10.015
5. Denning, C., V. Borgdorff, J. Crutchley, K.S. Firth, V. George, S. Kalra, A. Kondrashov, M.D. Hong, D. Mosqueira, A. Patel, et al. 2016. Cardiomyocytes from human pluripotent stem cells: From laboratory curiosity to industrial biomedical platform. Biochim. Biophys. Acta. 1863: 1728–1748. https://doi.org/10.1016/j.bbamcr.2015.10.014
6. Dostal, D.E., H. Feng, D. Nizamutdinov, H.B. Golden, S.H. Afroze, J.D. Dostal, J.C. Jacob, D.M. Foster, C. Tong, S. Glaser, and F. Gerilechaogetu. 2014. Mechanosensing and regulation of cardiac function. J. Clin. Exp. Cardiolog. 5:314, https://doi.org/10.4172/2155-9880.1000314
7. Gaetani, R., E.A. Zizzi, M.A. Deriu, U. Morbiducci, M. Pesce, and E. Messina. 2020. When stiffness matters: Mechanosensing in heart development and disease. Front. Cell Dev. Biol. 8:334. https://doi.org/10.3389/fcell.2020.00334
8. Haase, A., G. G¨ ohring, and U. Martin. 2017. Generation of non-transgenic iPS cells from human cord blood CD34+ cells under animal component-free conditions. Stem Cell Res. 21:71–73. https://doi.org/10.1016/j.scr.2017.03.022
9. Harvey, P.A., and L.A. Leinwand. 2011. The cell biology of disease: Cellular mechanisms of cardiomyopathy. J. Cell Biol. 194:355–365. https://doi.org/10.1083/jcb.201101100
10. Herron, T.J., E. Devaney, L. Mundada, E. Arden, S. Day, G. Guerrero-Serna, I. Turner, M. Westfall, and J.M. Metzger. 2010. Ca2+-independent positive molecular inotropy for failing rabbit and human cardiac muscle by alpha-myosin motor gene transfer. FASEB J. 24:415–424. https://doi.org/10.1096/fj.09-140566
11. Herron, T.J., and K.S. McDonald. 2002. Small amounts of alpha-myosin heavy chain isoform expression significantly increase power output of rat cardiac myocyte fragments. Circ. Res. 90:1150–1152. https://doi.org/10 .1161/01.RES.0000022879.57270.11
12. Herron, T.J., A.M. Rocha, K.F. Campbell, D. Ponce-Balbuena, B.C. Willis, G. Guerrero-Serna, Q. Liu, M. Klos, H. Musa, M. Zarzoso, et al. 2016. Extracellular matrix-mediated maturation of human pluripotent stem cell-derived cardiac monolayer structure and electrophysiological function. Circ. Arrhythm. Electrophysiol. 9:e003638. https://doi.org/10.1161/CIRCEP.113.003638
13. Herron, T.J., R. Vandenboom, E. Fomicheva, L. Mundada, T. Edwards, and J.M. Metzger. 2007. Calcium-independent negative inotropy by beta- myosin heavy chain gene transfer in cardiac myocytes. Circ. Res. 100 1182–1190. https://doi.org/10.1161/01.RES.0000264102.00706.4e
14. Iorga, B., K. Schwanke, N. Weber, M. Wendland, S. Greten, B. Piep, C.G. Dos Remedios, U. Martin, R. Zweigerdt, T. Kraft, and B. Brenner. 2018. Differences in contractile function of myofibrils within human embryonic stem cell-derived cardiomyocytes vs. Adult ventricular myofibrils are related to distinct sarcomeric proteinisoforms.Front.Physiol.8:1111. https://doi.org/10.3389/fphys.2017.01111
15. Israeli-Rosenberg, S., A.M. Manso, H. Okada, and R.S. Ross. 2014. Integrins and integrin-associated proteins in the cardiac myocyte. Circ. Res. 114: 572–586. https://doi.org/10.1161/CIRCRESAHA.114.301275
16. Jiang, Y., P. Park, S.M. Hong, and K. Ban. 2018. Maturation of cardiomyocytes derived from human pluripotent stem cells: Current strategies and limitations. Mol. Cells. 41:613–621. https://doi.org/10.14348/molcells.2018.014

17. Koc, A., S. Sahoglu Goktas, T. Akgul Caglar, and E. Cagavi. 2021. Defining optimal enzyme and matrix combination for replating of human induced pluripotent stem cell-derived cardiomyocytes at different levels of maturity. Exp. Cell Res. 403:112599. https://doi.org/10.1016/j.yexcr.2021.112599
18. Kraft, T., E.R. Witjas-Paalberends, N.M. Boontje, S. Tripathi, A. Brandis, J. Montag, J.L. Hodgkinson, A. Francino, F. Navarro-Lopez, B. Brenner et al. 2013. Familial hypertrophic cardiomyopathy: Functional effects of myosin mutation R723G in cardiomyocytes. J. Mol. Cell. Cardiol. 57: 13–22. https://doi.org/10.1016/j.yjmcc.2013.01.001
19. Kreutzer, F.P., A. Meinecke, S. Mitzka, H.J. Hunkler, L. Hobuß, N. Abbas, R. Geffers, J. Weusthoff, K. Xiao, D.D. Jonigk, et al. 2022. Development and characterisation of anti-fibrotic natural compound similars with improved effectivity. Basic Res. Cardiol. 117:9. https://doi.org/10.1007/s00395-022-00919-6
20. Leonard, A., A. Bertero, J.D. Powers, K.M. Beussman, S. Bhandari, M. Regnier, C.E. Murry, and N.J. Sniadecki. 2018. Afterload promotes maturation of human induced pluripotent stem cell derived cardiomyocytes in engineered heart tissues. J. Mol. Cell. Cardiol. 118:147–158. https://doi.org/10.1016/j.yjmcc.2018.03.016
21. Liao, Y., J. Wang, E.J. Jaehnig, Z. Shi, and B. Zhang. 2019. WebGestalt 2019: Gene set analysis toolkit with revamped UIs and APIs. Nucleic Acids Res. 47:W199–W205. https://doi.org/10.1093/nar/gkz401
22. Linke, W.A., and R.H. Kn¨ oll. 2010. Cardiac mechanosensation and clinical implications. Eur. J. Cardiovasc. Med. 1:33–37.
23. Locher, M.R., M.V. Razumova, J.E. Stelzer, H.S. Norman, J.R. Patel, and R.L. Moss. 2009. Determination of rate constants for turnover of myosin isoforms in rat myocardium: Implications for in vivo contractile kinetics. Am. J. Physiol. HeartCirc.Physiol.297:H247–H256. https://doi.org/10.1152/ajpheart.00922.2008
24. Lyon, R.C., F. Zanella, J.H. Omens, and F. Sheikh. 2015. Mechanotransduction in cardiac hypertrophy and failure. Circ. Res. 116:1462–1476. https://doi..org/10.1161/CIRCRESAHA.116.304937
25. Maltsev, V.A., A.M. Wobus, J. Rohwedel, M. Bader, and J. Hescheler. 1994. Cardiomyocytes differentiated in vitro from embryonic stem cells developmentally express cardiac-specific genes and ionic currents. Circ. Res. 75:233–244. https://doi.org/10.1161/01.RES.75.2.233
26. Molkentin, J.D., J.R. Lu, C.L. Antos, B. Markham, J. Richardson, J. Robbins, S.R. Grant, and E.N. Olson. 1998. A calcineurin-dependent transcriptional pathway for cardiac hypertrophy. Cell. 93:215–228. https://doi.org/10.1016/S0092-8674(00)81573-1
27. Münch, J., and S. Abdelilah-Seyfried. 2021. Sensing and responding of cardiomyocytes to changes of tissue stiffness in the diseased heart. Front. Cell Dev. Biol. 9:642840. https://doi.org/10.3389/fcell.2021.642840
28. Ng, R., L.R. Sewanan, P. Stankey, X. Li, Y. Qyang, and S. Campbell. 2021. Shortening velocity causes myosin isoform shift in human engineered heart tissues.Circ.Res.128:281–283. https://doi.org/10.1161/CIRCRESAHA.120.316950
29. Palmiter, K.A., M.J. Tyska, D.E. Dupuis, N.R. Alpert, and D.M. Warshaw. 1999. Kinetic differences at the single molecule level account for the functional diversity of rabbit cardiac myosin isoforms. J. Physiol. 519: 669–678. https://doi.org/10.1111/j.1469-7793.1999.0669n.x
30. Pentassuglia, L., and D.B. Sawyer. 2013. ErbB/integrin signaling interactions in regulation of myocardial cell-cell and cell-matrix interactions. Biochim. Biophys. Acta. 1833:909–916. https://doi.org/10.1016/j.bbamcr.2012.12.007
31. Pruna, M., and E. Ehler. 2020. The intercalated disc: A mechanosensing signalling node in cardiomyopathy. Biophys. Rev. 12:931–946. https://doi.org/10.1007/s12551-020-00737-x
32. Osten et al. Functional effects of replating hPSC-CMs Reiser, P.J., M.A. Portman, X.H. Ning, and C. Schomisch Moravec. 2001. Human cardiac myosin heavy chain isoforms in fetal and failing adult atria and ventricles. Am. J. Physiol. Heart Circ.Physiol.280:H1814–H1820. https://doi.org/10.1152/ajpheart.2001.280.4.H1814
33. Ren, X.D., R. Wang, Q. Li, L.A. Kahek, K. Kaibuchi, and R.A. Clark. 2004. Disruption of Rho signal transduction upon cell detachment. J. Cell Sci. 117:3511–3518. https://doi.org/10.1242/jcs.01205
34. Rundell, V.L., V. Manaves, A.F. Martin, and P.P. de Tombe. 2005. Impact of beta-myosin heavy chain isoform expression on cross-bridge cycling kinetics. Am. J. Physiol. Heart Circ. Physiol. 288:H896–H903. https://doi.org/10.1152/ajpheart.00407.2004
35. Sadoshima, J., and S. Izumo. 1997. The cellular and molecular response of cardiac myocytes to mechanical stress. Annu. Rev. Physiol. 59:551–571. https://doi.org/10.1146/annurev.physiol.59.1.551
36. Santoro, R., G.L. Perrucci, A. Gowran, and G. Pompilio. 2019. Unchain my heart: Integrins at the basis of iPSC cardiomyocyte differentiation. Stem Cells Int. 2019:8203950. https://doi.org/10.1155/2019/8203950
37. Saucerman, J.J., P.M. Tan, K.S. Buchholz, A.D. McCulloch, and J.H. Omens. 2019. Mechanical regulation of gene expression in cardiac myocytes and fibroblasts. Nat. Rev. Cardiol. 16:361–378. https://doi.org/10.1038/s41569-019-0155-8
38. Schwanke, K., S. Merkert, H. Kempf, S. Hartung, M. Jara-Avaca, C. Templin, G. G¨ ohring, A. Haverich, U. Martin, and R. Zweigerdt. 2014. Fast and efficient multitransgenic modification of human pluripotent stem cells. Hum. Gene Ther. Methods. 25:136–153. https://doi.org/10.1089/hgtb.2012..248

39. Schwartz, K., Y. Lecarpentier, J.L. Martin, A.M. Lompr´ e, J.J. Mercadier, and B. Swynghedauw. 1981. Myosin isoenzymic distribution correlates with speed of myocardial contraction. J. Mol. Cell. Cardiol. 13:1071–1075. https://doi.org/10.1016/0022-2828(81)90297-2
40. Weber, N., K. Kowalski, T. Holler, A. Radocaj, M. Fischer, S. Thiemann, J. de la Roche, K. Schwanke, B. Piep, N. Peschel, et al. 2020. Advanced single cell mapping reveals that in hESC-cardiomyocytes contraction kinetics and action potential are independent of myosin isoform. Stem Cell Rep. 14:788–802. https://doi.org/10.1016/j.stemcr.2020.03.015
41. Weber, N., K. Schwanke, S. Greten, M. Wendland, B. Iorga, M. Fischer, C. Geers-Kn¨ orr, J. Hegermann, C. Wrede, J. Fiedler, et al. 2016. Stiff matrix induces switch to pure β-cardiac myosin heavy chain expression in human ESC-derived cardiomyocytes. Basic Res. Cardiol. 111:68. https://doi.org/10.1007/s00395-016-0587-9
42. World Medical Association. 2013. World Medical Association Declaration of Helsinki: ethical principles for medical research involving human subjects. JAMA. 310:2191–2194. https://doi.org/10.1001/jama.2013.281053
43. Xu, X.Q., R. Zweigerdt, S.Y. Soo, Z.X. Ngoh, S.C. Tham, S.T. Wang, R. Graichen, B. Davidson, A. Colman, and W. Sun. 2008. Highly enriched cardiomyocytes from human embryonic stem cells. Cytotherapy. 10:376–389. https://doi.org/10.1080/14653240802105307
Yang, X., L. Pabon, and C.E. Murry. 2014. Engineering adolescence: Maturation of human pluripotent stem cell-derived cardiomyocytes. Circ.Res. 114:511–523. https://doi.org/10.1161/CIRCRESAHA.114.300558